International Journal of Bifurcation and Chaos, Vol. 30, No. 6 (2020) 2050086 (16 pages)

DOI: 10.1142/S0218127420500868

Four-Wing Hidden Attractors with One Stable Equilibrium Point

Quanli Deng*, Chunhua Wang† and Linmao Yang‡
College of Computer Science and Electronic Engineering,
Hunan University, Changsha 410082, P. R. China
*quanliden@hnu.edu.cn
†wch1227164@hnu.edu.cn
‡2640458643@qq.com

Received May 27, 2019; Revised September 5, 2019

Although multiwing hidden attractor chaotic systems have attracted a lot of interest, the currently reported multiwing hidden attractor chaotic systems are either with no equilibrium point or with an infinite number of equilibrium points. The multiwing hidden attractor chaotic systems with stable equilibrium points have not been reported. This paper reports a four-wing hidden attractor chaotic system, which has only one stable node-focus equilibrium point. The novel system can also generate a hidden attractor with one-wing and hidden attractors with quasi-periodic and periodic coexistence. In addition, a self-excited attractor with one-wing can be generated by adjusting the parameters of the novel system. The hidden attractors of the novel system are verified by the cross-section of attraction basins. And the hidden behavior is investigated by choosing different initial states. Moreover, the coexisting transient four-wing phenomenon of the self-excited one-wing attractor system is studied by the time domain waveforms and attraction basin. The dynamical characteristics of the novel system are studied by Lyapunov exponents spectrum, bifurcation diagram and Poincaré map. Furthermore, the novel hidden attractor system with four-wing and one-wing are implemented by electronic circuits. The hardware experiment results are consistent with the numerical simulations.

Keywords: Stable node-focus; four-wing attractor; coexisting attractors; attraction basin.

1. Introduction

Since Lorenz proposed the first simple three-dimensional chaotic system [Lorenz, 1963], chaos theory has established itself as an important branch of nonlinear dynamics with a broad range of applications in secure communication [Li *et al.*, 2009], image encryption [Zhou & Wang, 2020; Yin & Wang, 2018; Cheng *et al.*, 2019], cellular neural network [Lin & Wang, 2020; Yao *et al.*, 2019], etc. After the mathematical definition of hidden attractors was introduced by Leonov *et al.* [2011], the theory and application of studying hidden attractors have received extensive attention. The chaotic attractors can be classified as self-excited attractors and hidden attractors. For the hidden attractor, its attraction basin does not intersect any open neighborhood of the system equilibria, while the self-excited attractor's basin is associated with an unstable equilibrium. The widely-known chaotic attractors such as Lorenz attractor [Lorenz, 1963], Rössler attractor [Rössler, 1976] and Chen attractor [Chen & Ueta, 1999] belong as self-excited attractors because they are all excited from the unstable equilibrium points.

†Author for correspondence

From a computational point of view, hidden attractors can be classified into three categories: hidden attractor with stable equilibrium points, hidden attractor with no equilibrium point and hidden attractor with infinitely many equilibrium points. The first hidden chaotic attractor was found in a generalized Chua's circuit [Kuznetsov *et al.*, 2010], and the hidden attractor in the classical Chua's circuit was later reported in [Leonov *et al.*, 2011]. In 2010, Yang *et al.* [2010] proposed a generalized Lorenz chaotic system with two stable node-foci equilibrium points. Wang and Chen [2012] proposed a chaotic system with only one stable equilibrium point. Molaie *et al.* [2013] reported 23 simple chaotic flows with stable equilibrium point. The first hyperchaotic hidden attractor with stable equilibrium points was proposed by Wei and Zhang [2014]. Danca *et al.* [2016] discovered the hidden attractor with stable equilibrium points in the Rabinovich–Fabrikant system. Next year, Wei *et al.* [2017] reported a hyperchaotic hidden attractor in a 5D system. Cang *et al.* [2019], reported a Lorenz-like system with two equilibrium points, which has hidden attractors and self-excited coexisting attractors. Apart from the hidden attractors with stable equilibrium points, hidden attractors with no equilibrium point [Pham *et al.*, 2014; Pham *et al.*, 2017; Zhou *et al.*, 2018a] and hidden attractors with infinitely many equilibrium points [Jafari & Sprott, 2013; Zhou *et al.*, 2016; Wang *et al.*, 2018; Zhang & Wang, 2019b] were studied widely and deeply.

Compared with single-wing and two-wing attractor systems, multiwing attractor systems [Yu *et al.*, 2010a; Yu *et al.*, 2018; Yu *et al.*, 2012] and multiscroll attractor systems [Wang *et al.*, 2017a; Zhang & Wang, 2019a; Wang *et al.*, 2017b; Jin & Li, 2019; Jin, 2018] have more complex dynamic behaviors, making them more suitable for applications. The multiwing chaotic systems can be classified into two categories. The first type of multiwing chaotic systems is formed by smooth nonlinear functions. A 3D four-wing chaotic system with five equilibrium points was proposed in [Liu & Chen, 2003], and it was proved to be a pseudo four-wing chaotic system but consisted of two coexisting and closely located double-wing attractors in [Liu & Chen, 2004]. The real 3D four-wing attractors with five equilibrium points in a smooth autonomous system were proposed in [Lü *et al.*, 2004; Qi *et al.*, 2006]. Later, using the energy analysis, which has been used in many scenes [Qi & Yang, 2019; Qi, 2019], Qi *et al.* made a detailed analysis of the Qi four-wing attractor [Qi & Liang, 2017]. In 2012, Dadras *et al.* put forward a 4D hyperchaotic four-wing attractor with one unstable saddle equilibrium point for the first time [Dadras *et al.*, 2012]. A notable feature of these four-wing attractor chaotic systems, which consist of smooth nonlinear functions, is that the number of wings is not equal to that of equilibrium points. The other type of widely studied multiwing attractor chaotic system is constructed by introducing nonsmooth nonlinear parts into a chaotic system to increase the number of equilibrium points. Elwakil *et al.* [2003] proposed a four-wing butterfly attractor chaotic system by relying on two embedded state-controlled binary switches. Hereafter, nonsmooth nonlinear functions such as piecewise-linear function [Yu *et al.*, 2010b], heteroclinic loops [Yu *et al.*, 2011], multipiecewise square function [Ma *et al.*, 2017], etc. were applied to construct multiwing attractors or grid multiwing attractors. A notable feature of these multiwing attractor chaotic systems is that the nonlinear functions would increase the number of unstable equilibrium points, and the number of wings is equal to the number of equilibrium points.

The multiwing attractors mentioned above are self-excited, for all of them are excited from unstable equilibrium points. Tahir *et al.* [2015] constructed a multiwing butterfly attractor chaotic system with no equilibrium point. Zhou *et al.* [2017] constructed a four-wing hyperchaotic attractor and two-wing, three-wing and four-wing chaotic attractors with line equilibrium points (infinitely many equilibrium points) by introducing a memristor into a three-dimensional pseudo four-wing chaotic system. Zhang *et al.* [2018a] reported a 4D hidden attractor chaotic system with no-equilibrium point, which can generate one-wing to four-wing. In the same year, Zhang *et al.* [2018b] proposed a 4D no-equilibrium hyperchaotic system with grid multiwing hidden attractors. However, these multiwing hidden attractors belong to only two categories of hidden attractors of no-equilibrium point and an infinite number of equilibrium points. To the best of our knowledge, the multiwing hidden attractor with stable equilibrium points has not been reported. Here we construct a chaotic system, which can generate four-wing and one-wing hidden attractors with only one stable node-focus equilibrium point. Besides, the system has hidden attractors

with quasi-periodic and periodic coexistence, as well as a self-excited attractor with one-wing.

The paper is organized as follows. The formulation of the four-wing system is briefly introduced in Sec. 2. In Sec. 3, the dynamical behaviors of the system are discussed. The circuit implementation of the hidden attractors is carried out in Sec. 4. Some conclusions are finally drawn in Sec. 5.

2. The Four-Wing Hidden Attractor System

In this section, we propose a 4D system, which can generate a four-wing attractor and has only one equilibrium point. The state equations can be expressed as

$$\begin{cases} \dot{x} = ax - byz - 10, \\ \dot{y} = -cy + xz + kw, \\ \dot{z} = -dz + exy, \\ \dot{w} = f(x + z), \end{cases} \tag{1}$$

where a, b, c, d, e, f and k are positive parameters. In the following, some basic properties of the novel system are analyzed.

2.1. *Dissipation and existence of attractor*

The general case of the dissipation of system (1) is calculated as

$$\begin{aligned} \nabla V &= \frac{\partial \dot{x}}{\partial x} + \frac{\partial \dot{y}}{\partial y} + \frac{\partial \dot{z}}{\partial z} + \frac{\partial \dot{w}}{\partial w} \\ &= a - c - d. \end{aligned} \tag{2}$$

Thus, for $a < c + d$, system (1) is dissipative. It means that all orbits of the system converge to a specific subset of zero volume as $t \to \infty$ at an exponential rate ∇V, which is independent of system states. It is known that a volume element with its initial volume being V_0 can shrink to $V_0 e^{V_t}$, indicating that every volume element can shrink to a specific subset of zero with the exponential rate ∇V. Consequently, all system orbits can be limited to a point set of which the volume is zero, and its asymptotic motion forms an attractor.

2.2. *Equilibrium point and stability*

The equilibrium point of system (1) can be found by solving the following algebraic equations simultaneously

$$\begin{cases} ax - byz - 10 = 0, \\ -cy + xz + kw = 0, \\ -dz + exy = 0, \\ f(x + z) = 0. \end{cases} \tag{3}$$

From the fourth equation we can get the relationship of state variables x and z, which can be expressed as

$$x = -z. \tag{4}$$

Substituting Eq. (4) into the third equation of Eq. (3), we can get that the value of state variable y equals to $-d/e$. Substituting Eq. (4) and the value of state variable y into the first and the second equations of Eq. (3), we can get that the values of state variables x, z and w can be expressed as

$$\begin{cases} x = -z = \dfrac{10}{a - b\left(\dfrac{d}{e}\right)}, \\ w = \dfrac{-c\left(\dfrac{d}{e}\right) + \left(\dfrac{10}{a - b\left(\dfrac{d}{e}\right)}\right)^2}{k}. \end{cases} \tag{5}$$

Hence, the only equilibrium point of system (1) is

$$E^* \begin{cases} x^* = \dfrac{10}{a - b\left(\dfrac{d}{e}\right)}, \\ y^* = -\dfrac{d}{e}, \\ z^* = -\dfrac{10}{a - b\left(\dfrac{d}{e}\right)}, \\ w^* = \dfrac{-c\left(\dfrac{d}{e}\right) + \left(\dfrac{10}{a - b\left(\dfrac{d}{e}\right)}\right)^2}{k}. \end{cases} \tag{6}$$

The Jacobian matrix at the equilibrium point can be expressed as

$$J(E^*) = \left[\begin{matrix} a & -bz & -by & 0 \\ z & -c & x & k \\ ey & ex & -d & 0 \\ f & 0 & f & 0 \end{matrix}\right]\Bigg|_{E^*}. \tag{7}$$

The stability of E^* is determined by the eigenvalues of Eq. (7). In this part, we set the parameters to $b = 6$, $c = 10$, $e = 2$, $f = 0.05$ and $k = 2.5$, to investigate the effect of parameters a and d on the stability of the equilibrium point. Equation (7) can be rewritten as follows

$$J(E^*) = \begin{bmatrix} a & -\dfrac{60}{a-3d} & 3d & 0 \\ -\dfrac{10}{a-3d} & -10 & \dfrac{10}{a-3d} & 2.5 \\ -d & \dfrac{20}{a-3d} & -d & 0 \\ 0.05 & 0 & 0.05 & 0 \end{bmatrix}. \tag{8}$$

It is tough to judge the stability of E^* by the characteristic equation of the Jacobian matrix (8). We use the numerical simulation method to investigate the effects of changing parameters a and d from 1 to 10 on the stability of E^*. Figure 1 shows the results of the numerical simulation. The green region in Fig. 1 indicates that a stable equilibrium point E^* can be obtained by selecting the corresponding parameters a and d. The red region represents the region of parameters a and d corresponding to the unstable equilibrium points.

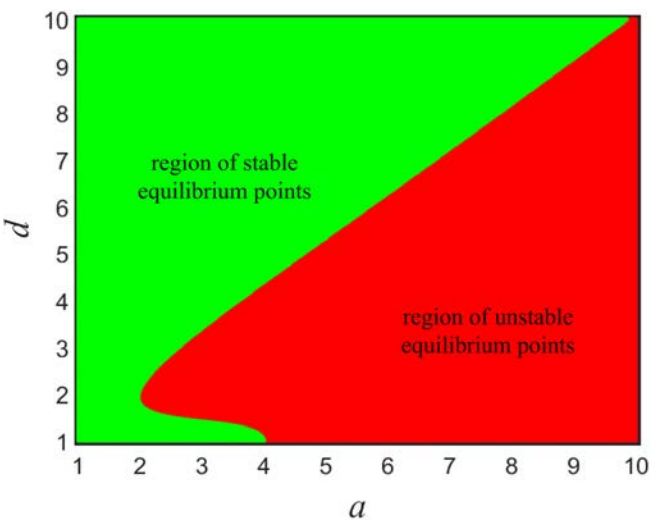

Fig. 1. Classification of stability of the equilibrium points by parameters a and d, setting $b = 6$, $c = 10$, $e = 2$, $f = 0.05$ and $k = 2.5$.

3. Dynamical Behaviors of the New System

3.1. *Four-wing hidden attractor*

In this subsection, the numerical simulations are carried out by performing the fourth Runge–Kutta integration algorithm, using MATLAB program. Fix $b = 6$, $c = 10$, $e = 2$, $f = 0.05$, $k = 2.5$ and set $a = 4$, $d = 5$. The system (1) can generate a four-wing attractor with the initial values $(-0.91, -2.3, 0.91, 1)$. Phase portraits of the four-wing attractor are shown in Fig. 2.

Substituting the parameters into Eq. (6), we can get that the equilibrium point of the system is

$$E^*(-0.91, -2.5, 0.91, -9.7). \tag{9}$$

The Jacobian matrix of system (1) at the equilibrium point can be expressed as

$$J(E^*) = \begin{bmatrix} a & -bz & -by & 0 \\ z & -c & x & k \\ ey & ex & -d & 0 \\ f & 0 & f & 0 \end{bmatrix}\Bigg|_{E^*} = \begin{bmatrix} 4 & -\dfrac{60}{11} & 15 & 0 \\ \dfrac{10}{11} & -10 & -\dfrac{10}{11} & 2.5 \\ -5 & -\dfrac{20}{11} & -5 & 0 \\ 0.05 & 0 & 0.05 & 0 \end{bmatrix}. \tag{10}$$

So, the eigenvalues of the system (1) at the equilibrium point are $\lambda_1 = -10.311$, $\lambda_2 = -0.0004$, $\lambda_{3,4} = -0.3406 \pm 7.8189i$. The only equilibrium point E^* is a stable node-focus, which means the motion starting from the neighborhood of E^* will converge to it. However, Fig. 2 displays a four-wing chaotic attractor generated by the stable equilibrium point E^*. This implies that the four-wing attractor is a hidden attractor.

An attractor is called a hidden attractor if its basin of attraction does not intersect with any open neighborhood of the system equilibria, otherwise, it is called a self-excited attractor [Leonov *et al.*, 2011]. The attraction basin is defined as the set of initial conditions that lead to a given attractor.

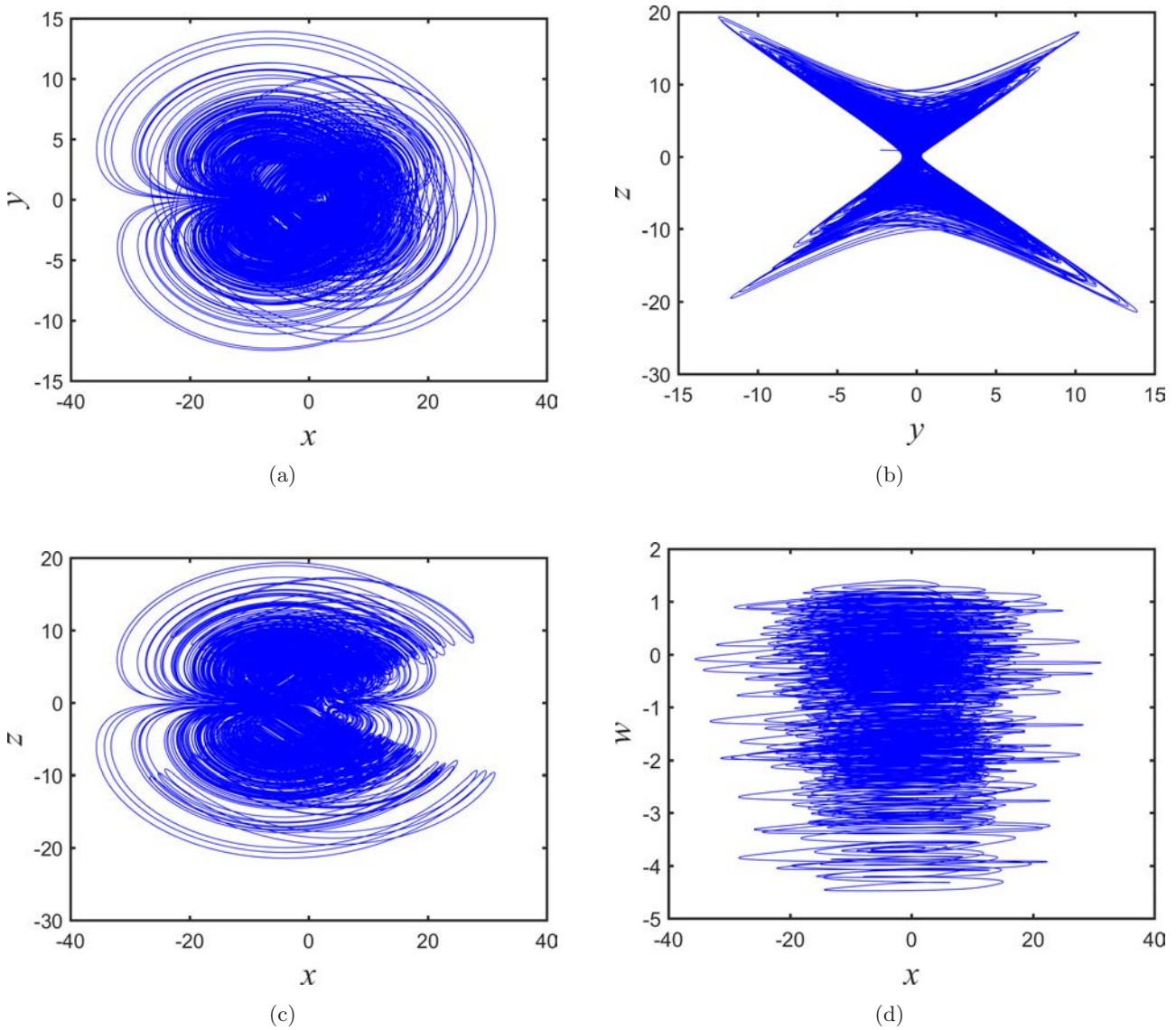

Fig. 2. Phase portraits of four-wing attractor in (a) x–y plane, (b) y–z plane, (c) x–z plane and (d) x–w plane.

Using the numerical simulation method [Chen *et al.*, 2019; Li *et al.*, 2018a] to classify the initial conditions corresponding to the different attractor types, we can get the attraction basins. To reflect the relationship of the attraction basins, we use different colors to represent the basins of different types of attractors. To check whether the attraction basin intersects with the small neighborhood of equilibrium point E^*, a section plane $\{x = -0.91, y, z = 0.91, w\}$ is chosen to pass through the stable equilibrium point. As shown in Fig. 3, the red dot denotes the equilibrium point, two types of attraction basins are marked in cyan and blue, respectively. The cyan region in Fig. 3 denotes the attraction basin of the chaotic attractor. The blue region represents that the motions starting from this initial state region will converge to the equilibrium point (called the point attractor). It can be seen from Fig. 3 that the attraction basin of the chaotic attractor does not intersect with the stable equilibrium point. Based on the analysis of the cross-section of the attraction basin, we can determine the four-wing attractor as a hidden attractor. Moreover, we select two initial states, $initial1(-0.9, -10.8, 0.9, 6)$ and $initial2(-0.9, -8.8, 0.9, -6.6)$, to explore the hidden chaotic behavior of the four-wing attractor. The two initial states are selected in the attraction basin's cross-section plane that passes through the

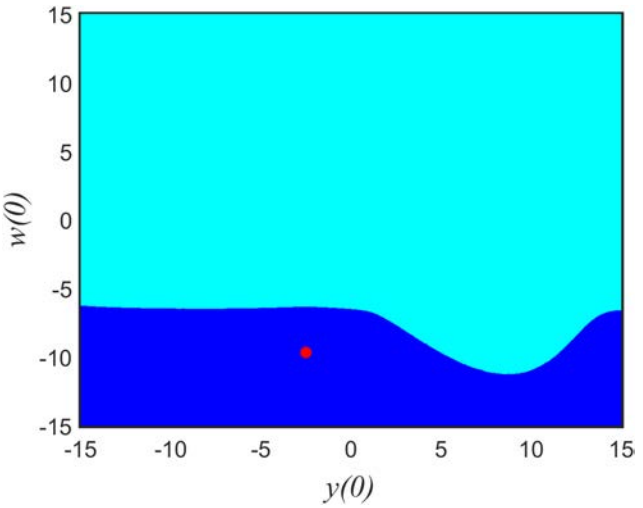

Fig. 3. Cross-section $x = -0.91$, y, $z = 0.91$, w of attraction basin.

equilibrium point. The *initial*1 is in the attraction basin of the four-wing attractor. And the *initial*2 is in the attraction basin of the point attractor. Figure 4 shows the 3D view of the phase portrait with the two initial states. From Fig. 4, we can see that the motion starting from *initial*1 is chaotic. However, the motion starting from *intial*2 converges to the equilibrium point represented by the blue dot. From a computational point of view, the four-wing attractor cannot be identified by the numerical method in which a trajectory starts from a point on the unstable manifold in the neighborhood of the equilibrium point. In other words, the dynamic behaviors also illustrate that the four-wing attractor is a hidden attractor.

The phase space of some nonlinear systems can become overcrowded and the underlying structure

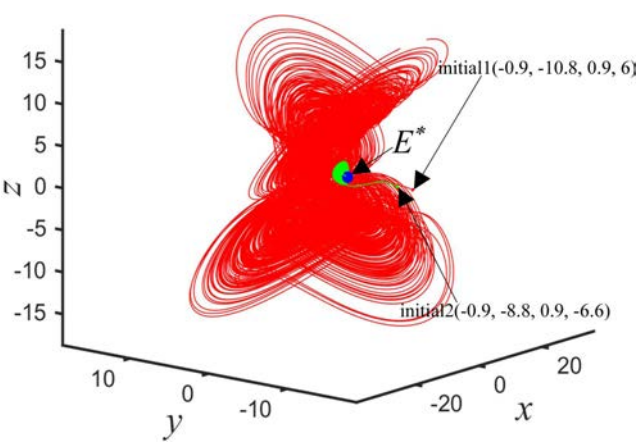

Fig. 4. 3D view of phase portrait with initial states: *initial*1 $(-0.9, -10.8, 0.9, 6)$ and *initial*2$(-0.9, -8.8, 0.9, -6.6)$.

may become obscured. Poincaré map can be used to overcome these difficulties. It is often used to reduce a higher-dimensional continuous system to a discrete map of the lower dimension. In this way, it can demonstrate the bifurcating and folding planes in a system. Figure 5 shows the Poincaré map of four-wing hidden attractor by setting parameters $a = 4$, $b = 6$, $c = 10$, $d = 5$, $e = 2$, $f = 0.05$ and $k = 2.5$ with initial states $(-0.91, -2.3, 0.91, 1)$. As can be seen from Fig. 5, the Poincaré maps here consist of four or six branches, which imply that the orbits of the attractor are continuously folded and bifurcated in different directions.

3.2. *One-wing hidden attractor*

Fix $b = 6$, $c = 10$, $e = 2$, $f = 0.05$, $k = 2.5$ and set $a = 3$, $d = 4$. The equilibrium point can be calculated as

$$E^*(-0.91, -2, 0.91, -7.5). \tag{11}$$

The eigenvalues at the equilibrium point are $\lambda_1 = -10.347$, $\lambda_2 = -0.0054$ and $\lambda_{3,4} = -0.323 \pm 6.639i$. It is a stable node-focus equilibrium point. Figure 6 shows the phase portraits of one-wing attractor generated by system (1) under such parameters.

Figure 7(a) displays the section plane $\{x = -1.1, y, z = 1.1, w\}$ of attraction basin, which passes through the equilibrium point. As shown in Fig. 7(a), the red dot denotes the equilibrium point, the attraction basin of the chaotic attractor is marked in cyan and the attraction basin of the point attractor is marked in blue. The mixed region at the boundary indicates that the initial conditions selected from here may result in either a chaotic attractor or a point attractor. As can be seen from Fig. 7(a), the equilibrium point does not connect with the chaotic attraction basin. However, the equilibrium point is located in the blue region representing the point attractor. We can get that the cross-section of the chaotic attraction basin does not intersect with the equilibrium point. So, we can determine the one-wing attractor as a hidden attractor. The hidden chaotic behavior of the one-wing attractor is also studied by two initial states, *initial*1$(-1.11, -3.72, 1.11, -0.62)$ and *initial*2$(-1.11, -4.72, 1.11, -4.85)$. The two initial states are selected in the attraction basin's cross-section plane that passes through the equilibrium point. The *initial*1 is in the attraction basin of the one-wing attractor. And the *initial*2 is in the

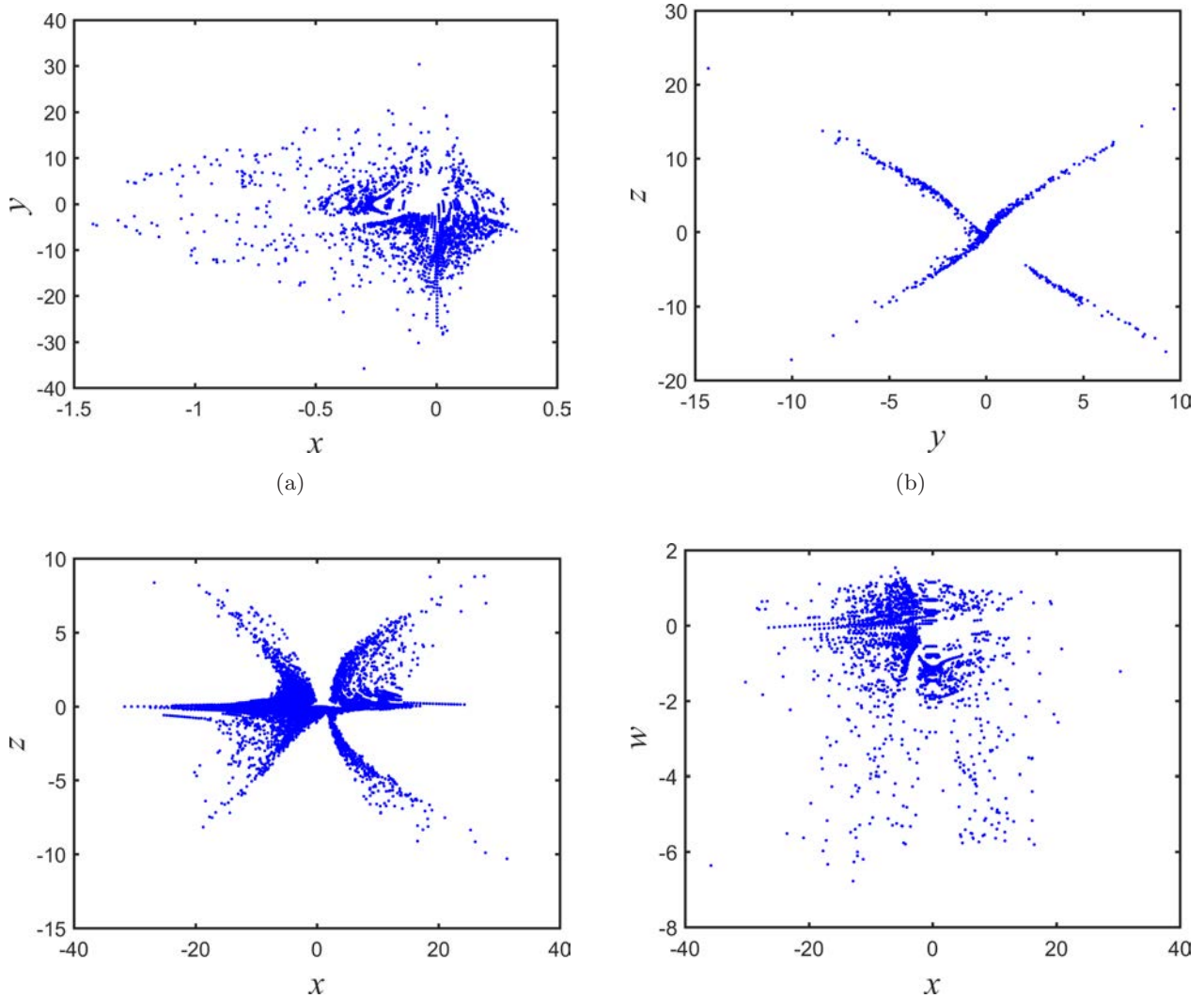

Fig. 5. Poincaré maps of four-wing hidden attractor in (a) x–y plane, (b) y–z plane, (c) x–z plane and (d) x–w plane.

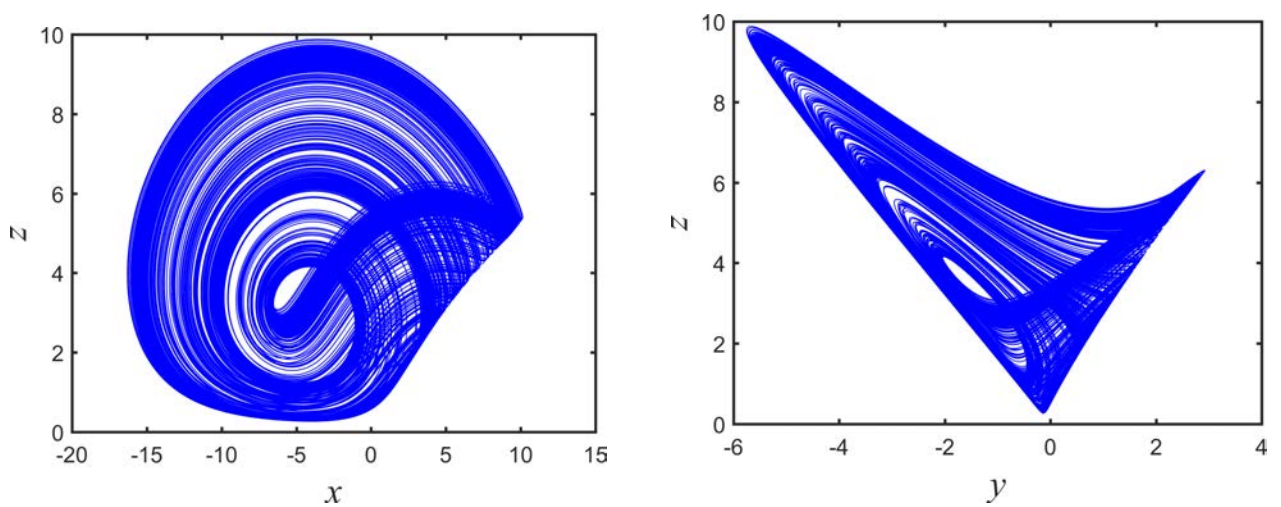

Fig. 6. Phase portraits of one-wing attractor in (a) x–z plane, (b) y–z plane, (c) x–y plane and (d) x–w plane.

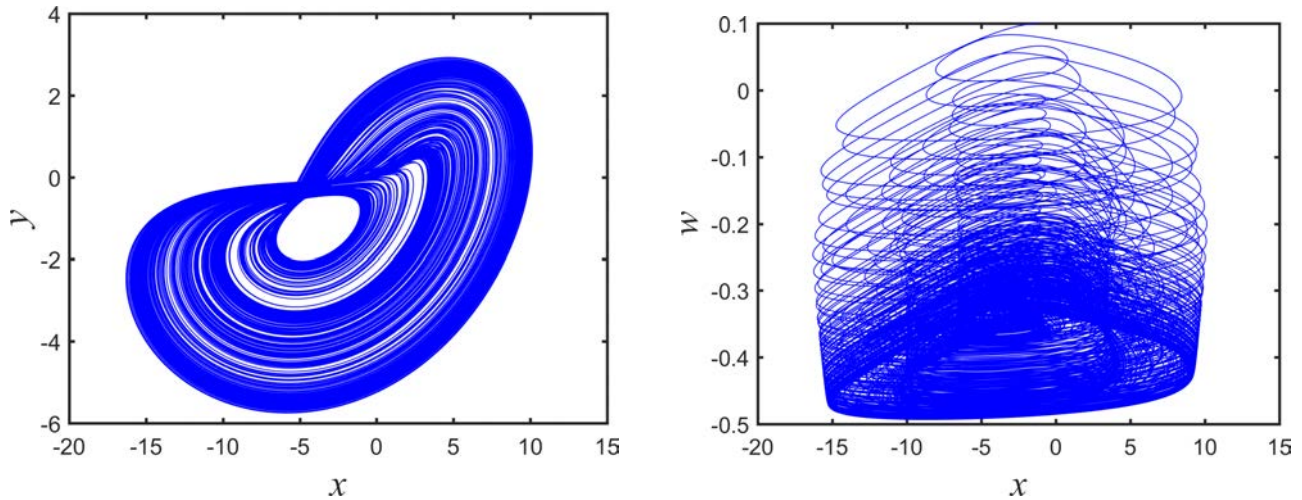

(c) (d)

Fig. 6. (*Continued*)

attraction basin of the point attractor. Figure 7(b) shows the 3D view of the phase portrait. From Fig. 7(b), we can see that the motion starting from *initial*1 is chaotic, while the motion starting from the *initial*2 converges to the equilibrium point. From a computational point of view, we can identify the one-wing attractor as a hidden attractor.

3.3. *Coexisting hidden attractor with quasi-period and period*

The coexistence of many different attractors for the same system parameters, has become a very striking and important research topic [Zhou *et al.*, 2018b; Li *et al.*, 2018b; Li *et al.*, 2019a; Li *et al.*, 2019b]. Fix $b = 6$, $c = 10$, $e = 2$, $f = 0.05$, $k = 2.5$ and set $a = 3$, $d = 7$. The equilibrium point can be calculated as

$$E^*(-0.56, -3.5, 0.56, -13.9). \tag{12}$$

The eigenvalues at the equilibrium point are $\lambda_1 = -10.151$, $\lambda_2 = -0.0019$ and $\lambda_{3,4} = -1.923 \pm 11.156i$. Under such parameters, system (1) generates attractors with quasi-periodic and periodic coexistence. Figure 8(a) is the phase portrait in y–z plane of quasi-periodic with initial state *initial*1$(-0.555, -3.15, 0.555, 1.28)$. Figure 8(b) is the corresponding time series of state variable z.

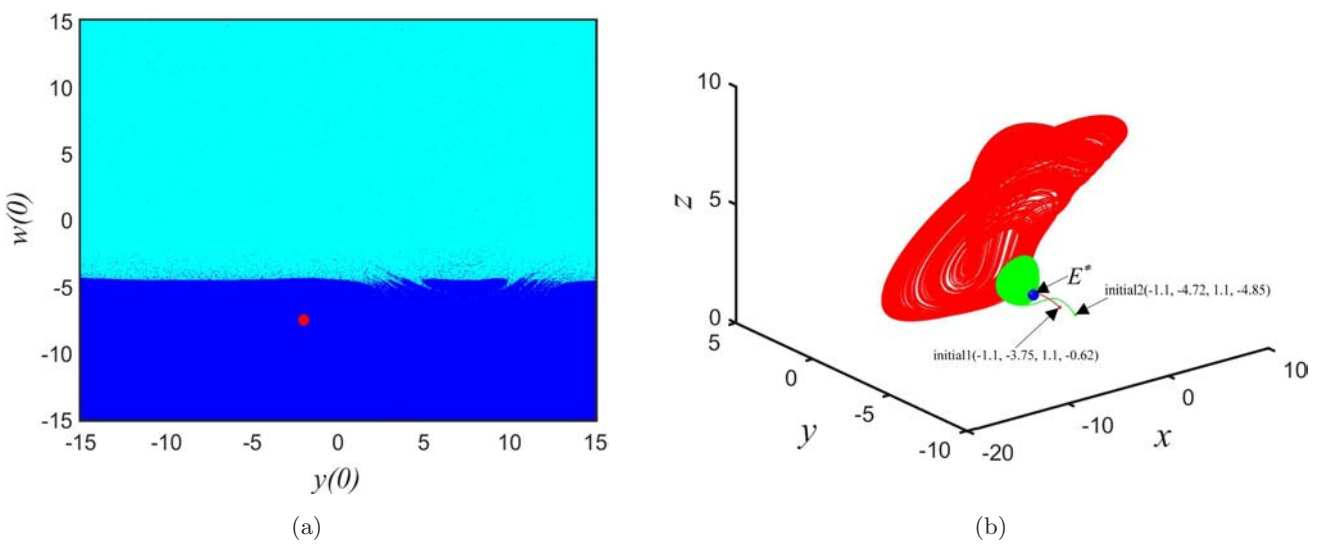

(a) (b)

Fig. 7. (a) Cross-section of attraction basin and (b) 3D view of phase portrait with initial states: *initial*1$(-1.11, -3.72, 1.11, -0.62)$ and *initial*2$(-1.11, -4.72, 1.11, -4.85)$.

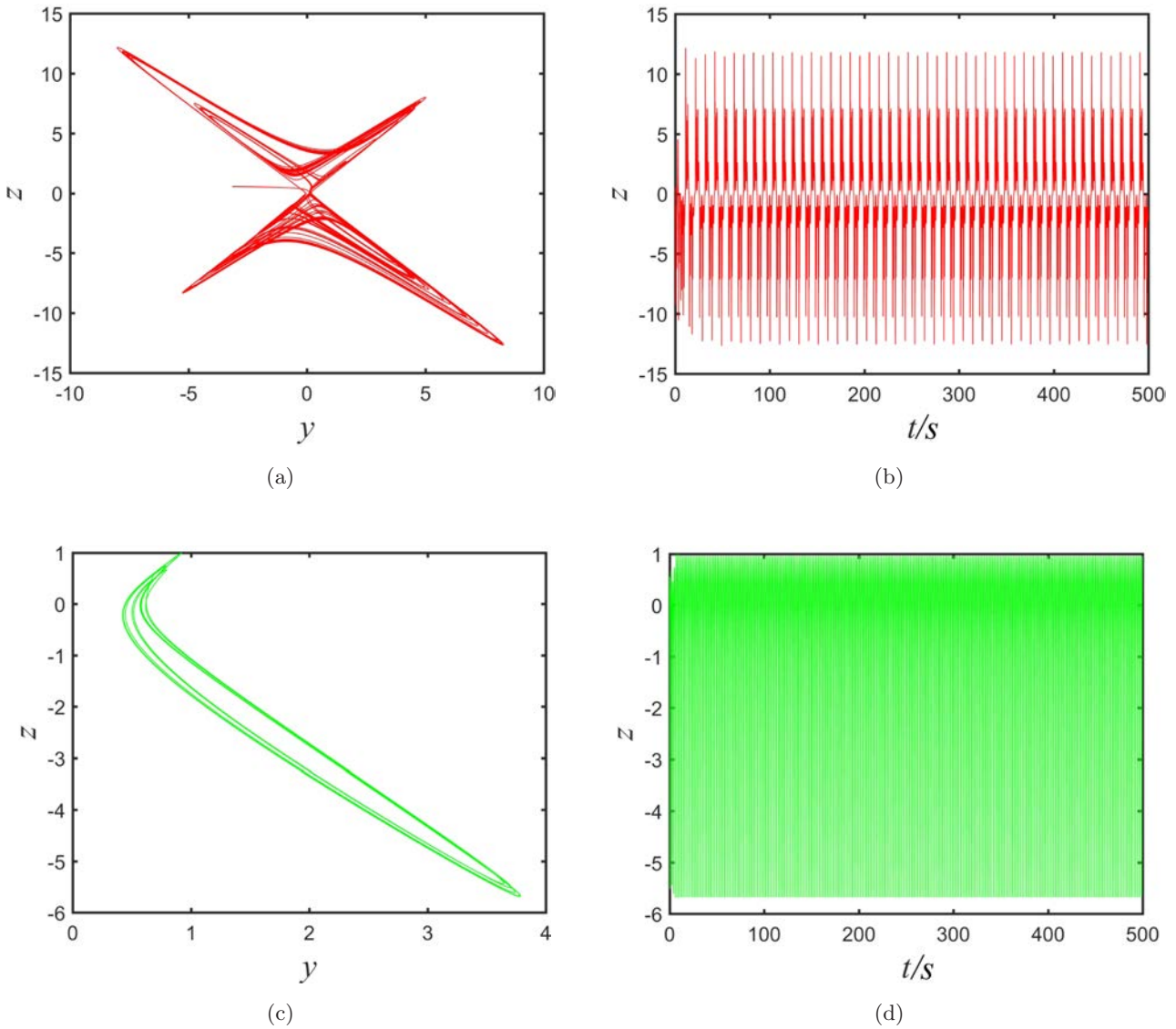

Fig. 8. (a) Phase portrait of quasi-periodic attractor in y–z plane, (b) time series of quasi-periodic attractor of state variable z, (c) phase portrait of periodic attractor in y–z plane and (d) time series of periodic attractor of state variable z.

The Lyapunov exponents of the quasi-periodic attractor are $\mathrm{LE}_1 = 0.022$, $\mathrm{LE}_2 = -0.025$, $\mathrm{LE}_3 = -0.138$ and $\mathrm{LE}_4 = -13.858$. Figure 8(c) shows the phase portrait in y–z plane of periodic attractor with initial state $initial2(-0.555, 0.68, 0.555, 2.53)$. Figure 8(d) shows the corresponding time series of state variable z. The Lyapunov exponents of the periodic attractor are $\mathrm{LE}_1 = -0.0006$, $\mathrm{LE}_2 = -0.446$, $\mathrm{LE}_3 = -0.462$ and $\mathrm{LE}_4 = -13.090$.

Figure 9 shows the cross-section plane $\{x = -0.56, y, z = 0.56, w\}$ of attraction basin, which passes through the equilibrium point denoted by the red dot. The blue region in Fig. 9 denotes the attraction basin of point attractor, the yellow regions denote quasi-periodic attractor, and the cyan region denotes periodic attractor. The blue and cyan dots filling the yellow region indicate that the initial conditions selected from here may result in any point attractor, a quasi-periodic attractor or a periodic attractor. Based on Fig. 9, we can determine that the quasi-periodic attractor and the periodic attractor are hidden attractors because their attraction basins do not intersect with the equilibrium point.

3.4. *Self-excited one-wing attractor and transient four-wing phenomenon*

Fix $b = 6$, $c = 10$, $e = 2$, $f = 0.05$, $k = 2.5$, and set $a = 3$, $d = 3$. The equilibrium point can be

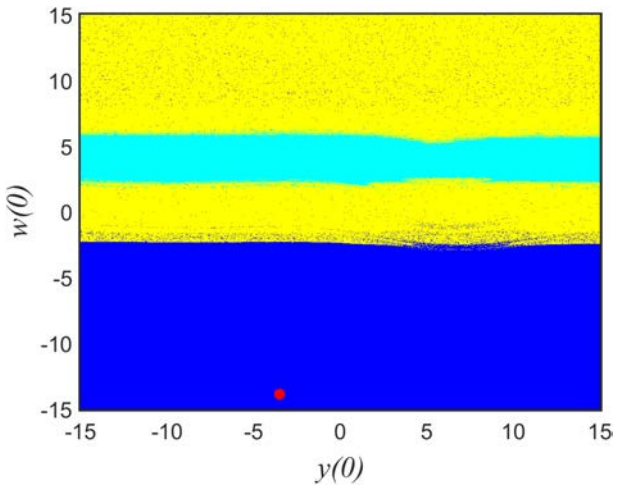

Fig. 9. 3D view of phase portrait with initial states: $initial1(-10/11, -10.8, 10/11, 6)$ and $initial2(-10/11, -8.8, 10/11, -6.6)$.

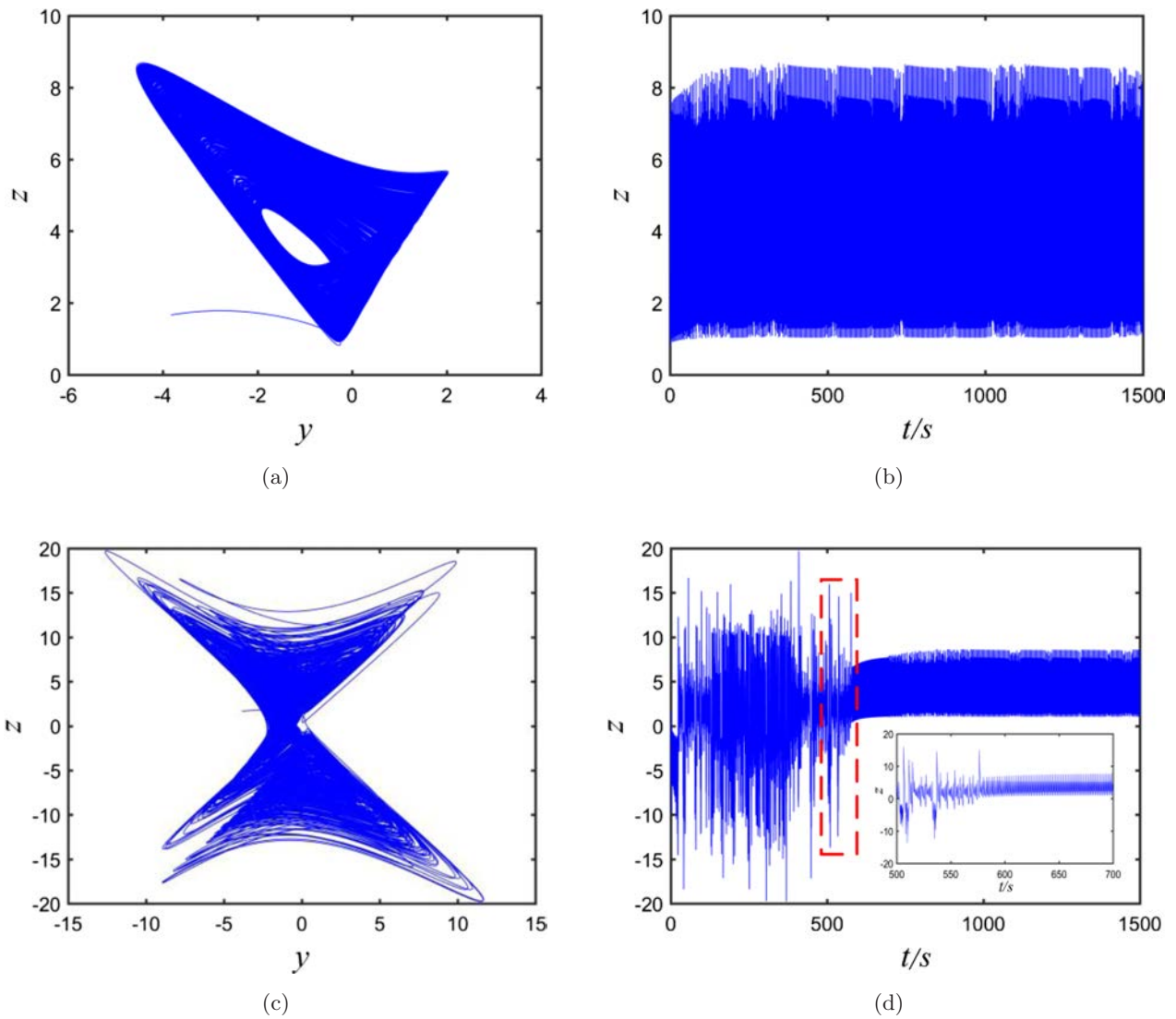

Fig. 10. (a) Phase portrait of one-wing self-excited attractor in y–z plane, (b) time domain waves of state variable z, (c) phase portrait of transient four-wing self-excited attractor in y–z plane and (d) time domain waves of transient four-wing phenomenon.

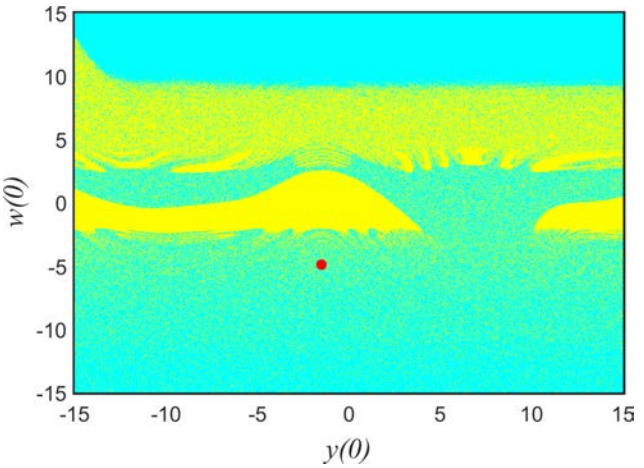

Fig. 11. Attraction basin of one-wing and transient four-wing attractor.

calculated as

$$E^*(-1.67, -1.5, 1.67, -4.9). \tag{13}$$

The eigenvalues at the equilibrium point are $\lambda_1 = -10.414$, $\lambda_2 = -0.007$ and $\lambda_{3,4} = 0.211 \pm 5.778i$. It is an unstable saddle-focus equilibrium point for which the eigenvalues have positive parts. By such parameters setting, system (1) generates a one-wing chaotic attractor with initial state $initial1((-1.667, -3.83, 1.667, 0.01)$. Figures 10(a) and 10(b) show the phase portrait of the one-wing attractor in y–z plane and the time domain waves of state variable z. In addition, there exist many initial state regions, in which transient four-wing attractor can be generated. We take initial state $initial2(-1.667, -3.83, 1.667, 2.18)$ as an example to display the transient phenomenon. Figures 10(c) and 10(d) are the corresponding phase portrait of the transient four-wing attractor in y–z plane and the time domain waves of state variable z. From Fig. 10(d), we can see that the time domain waves corresponding to the four-wing attractor last for around 550 s, and then the time domain waves become the form of the one-wing attractor.

To investigate the initial regions of transient four-wing attractor, we select a cross-section plane $\{x = -1.67, y, z = 1.67, w\}$ of attraction basin, which passes through the equilibrium point denoted by the red dot. These cyan regions in Fig. 11 denote attraction basins of the one-wing attractor, while these yellow ones denote attraction basins of the transient four-wing attractor. Most regions of the two attraction basins are intertwined. The initial conditions chosen from the intertwined regions may result in either of a one-wing attractor or a transient four-wing attractor. As can be seen in the figure, these chaotic attractors are self-excited, because the attraction basins of chaotic attractors intersect with the unstable equilibrium point.

3.5. *Lyapunov spectrum and bifurcation diagram*

For further investigating the dynamics of system (1), the controlled bifurcation parameter d is changed from 1 to 9, while the other parameters are fixed as $a = 3$, $b = 6$, $c = 10$, $e = 2$, $f = 0.05$ and $k = 2.5$. We can get the corresponding spectrum of Lyapunov exponents, as shown in Fig. 12(a), and

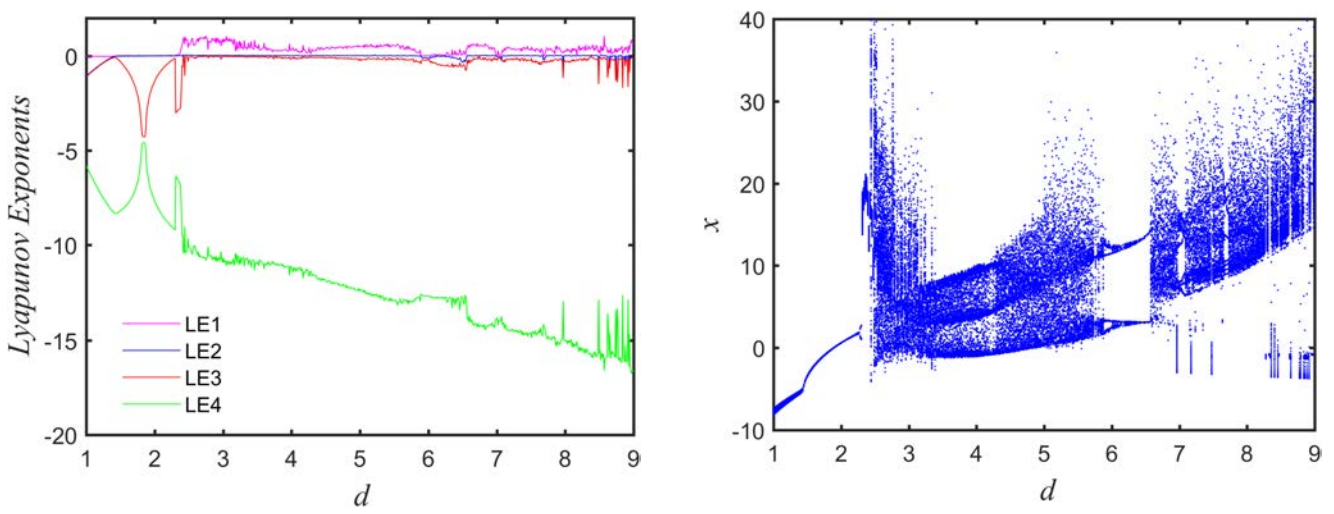

(a) (b)

Fig. 12. (a) Lyapunov exponent spectra versus parameter d and (b) corresponding bifurcation diagram of state variable x.

Table 1. The dynamics of system with respect to parameter d.

d	(LE_1, LE_2, LE_3, LE_4)	Dynamic
$[1, 1.36)$	$(0, -, -, -)$	Periodic orbits
$[1.36, 2.36)$	$(0, 0, -, -)$	Torus
$[2.36, 5.94)$	$(+, 0, -, -)$	Chaos
$[5.94, 6.12)$	$(0, -, -, -)$	Periodic orbits
$[6.12, 6.4)$	$(0, 0, -, -)$	Torus
$[6.4, 6.54)$	$(0, -, -, -)$	Periodic orbits
$[6.54, 9)$	$(+, 0, -, -)$	Chaos

the bifurcation diagram of state variable x, as shown in Fig. 12(b). From Fig. 12(a), we can observe that the system has complex dynamic behaviors such as chaos, torus, and periodic orbits. Most of the dynamical systems can be characterized by their Lyapunov exponents, which are classified in Table 1. The bifurcation behaviors, shown in Fig. 12(b), match the analysis of Lyapunov exponents.

4. Circuit Experiment

In this part, a circuit, which can generate hidden attractors is designed. And the hardware circuit is implemented by using TL082 op-amps. Their supply voltages are $\pm 15\,\mathrm{V}$ and the saturation voltage is around $13.5\,\mathrm{V}$. All the multipliers are selected as AD633JN, whose voltage gain is 0.1. The implementation circuit is shown in Fig. 13.

According to Fig. 2, the phase portrait, the state variable values are out of the saturation range of op-amps. Reducing the state variable values five times, we can get that the system can be expressed as

$$\begin{cases} \dot{x} = ax - 5byz - \dfrac{10}{5}, \\ \dot{y} = -cy + 5xz + kw, \\ \dot{z} = -dz + 5exy, \\ \dot{w} = f(x + z). \end{cases} \tag{14}$$

Now, using the voltage across the capacitance V_{c1}, V_{c2}, V_{c3} and V_{c4} represents the variable values x, y, z and w. The differential function can be changed as

$$\begin{cases} C_1 \dfrac{dx}{dt} = -\dfrac{1}{R_1} V_1 + \dfrac{1}{R_2} x - \dfrac{1}{10R_3} yz, \\ C_2 \dfrac{dy}{dt} = -\dfrac{1}{R_4} y + \dfrac{1}{R_5} w + \dfrac{1}{10R_6} xz, \\ C_3 \dfrac{dz}{dt} = -\dfrac{1}{R_7} z + \dfrac{1}{10R_8} xy, \\ C_4 \dfrac{dw}{dt} = \dfrac{1}{R_9} z + \dfrac{1}{R_{10}} x. \end{cases} \tag{15}$$

We select the values of capacitors as follows: $C_1 = C_2 = C_3 = C_4 = 10\,\mathrm{nF}$. According to the

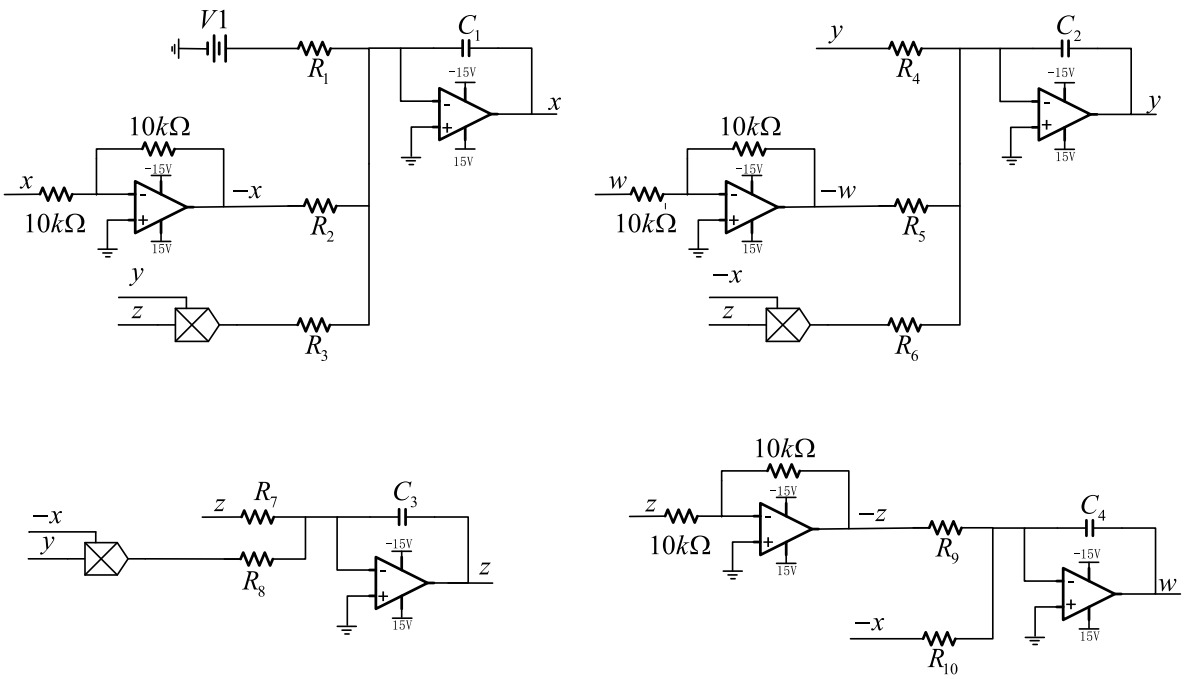

Fig. 13. Circuit diagram of the novel system.

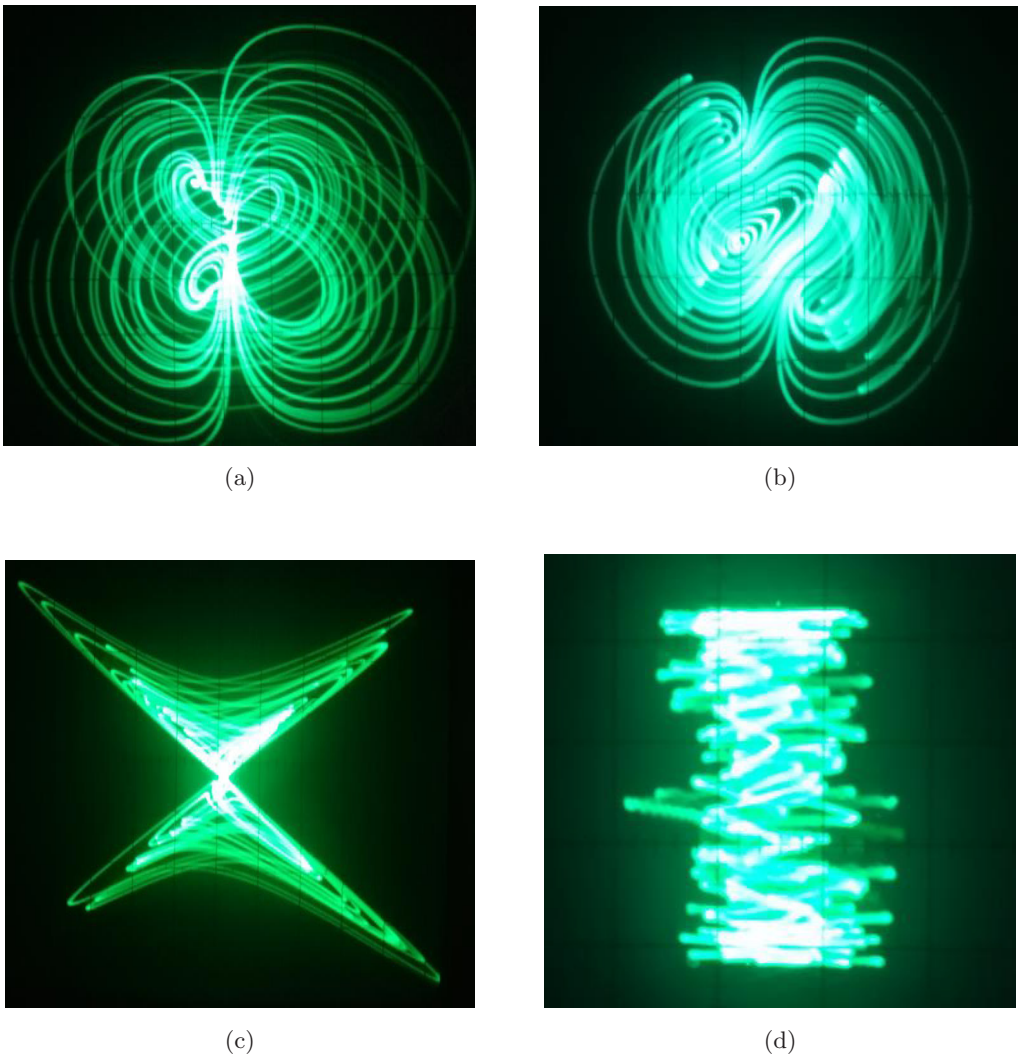

(a) (b)

(c) (d)

Fig. 14. Phase portraits of the four-wing hidden chaotic system in (a) x–y plane, (b) x–z plane, (c) y–z plane and (d) x–w plane.

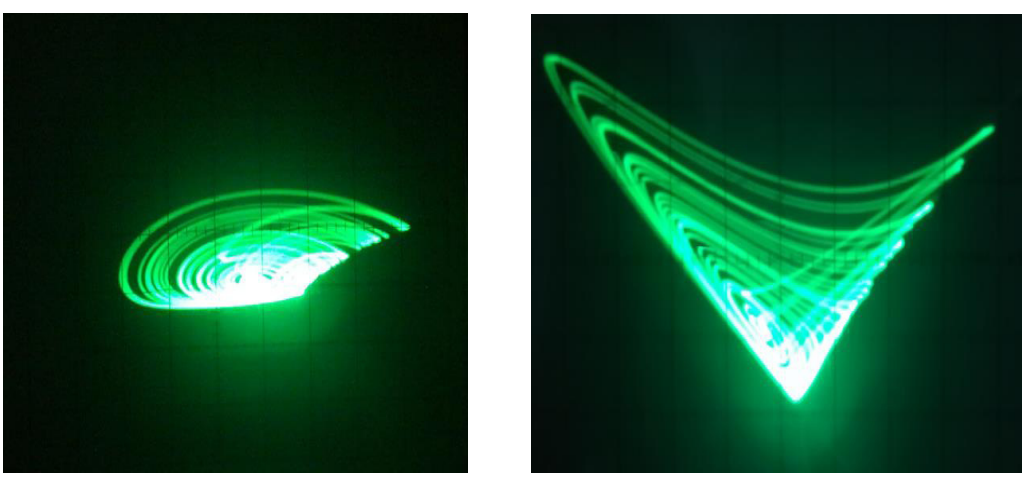

(a) (b)

Fig. 15. Phase portraits of the one-wing hidden chaotic system in (a) x–z plane, (b) y–z plane, (c) x–y plane and (d) x–w plane.

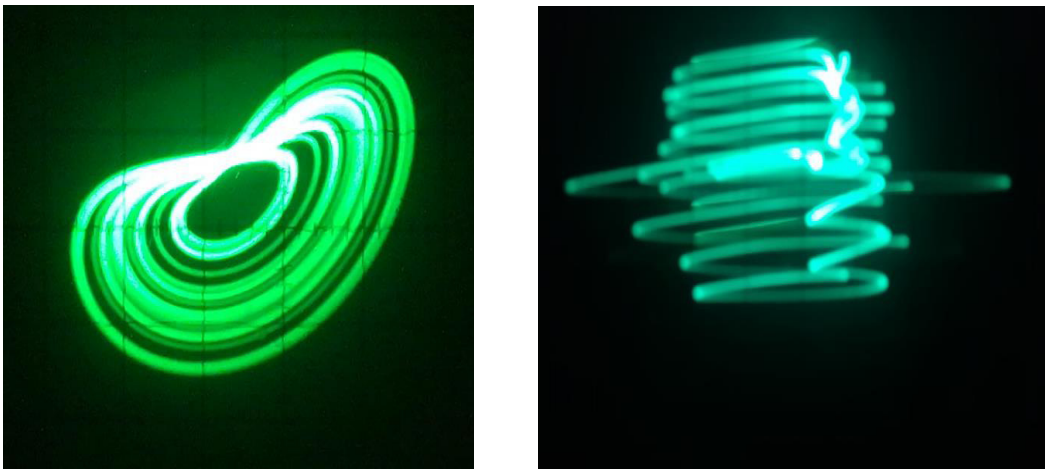

(c) (d)

Fig. 15. (*Continued*)

parameters of the four-wing hidden attractor, we take $R_1 = 5\,\mathrm{M}\Omega$, $R_2 = 250\,\mathrm{k}\Omega$, $R_3 = 3.33\,\mathrm{k}\Omega$, $R_4 = 100\,\mathrm{k}\Omega$, $R_5 = 400\,\mathrm{k}\Omega$, $R_6 = 20\,\mathrm{k}\Omega$, $R_7 = 200\,\mathrm{k}\Omega$, $R_8 = 10\,\mathrm{k}\Omega$ and $R_9 = R_{10} = 20\,\mathrm{M}\Omega$. The DC voltage V_1 is set to 10 V. Figure 14 shows the phase portraits of the four-wing hidden attractor. Considering parameters of one-wing hidden attractor $a = 3$, $b = 6$, $c = 10$, $d = 4$, $e = 2$, $f = 0.05$ and $k = 2.5$, changing the resistors $R_2 = 333\,\mathrm{k}\Omega$ and $R_7 = 250\,\mathrm{k}\Omega$, while keeping others fixed, the one-wing hidden attractor can be generated. The phase portraits of one-wing hidden attractor are shown in Fig. 15.

5. Conclusion

In this paper, we present a four-wing hidden attractor system with only one stable equilibrium point. In addition, the novel system can also generate a one-wing chaotic hidden attractor and quasi-periodic and periodic coexistence hidden attractors. And a self-excited one-wing attractor can be generated by setting different parameters. Performances of the hidden attractor are investigated by phase portraits, cross-section of attraction basin, Lyapunov exponents spectrum, bifurcation diagram and Poincaré map. The transient phenomenon in the self-excited one-wing attractor system is studied by time domain waves and attraction basin. The hardware experiment of the proposed system is carried out. It is believed that the proposed novel system will contribute to the development of theoretical study of multiwing hidden attractors.

Acknowledgments

This work is supported by the National Natural Science Foundation of China (No. 61971185), Research Plan of the National Natural Science Foundation of China (No. 91964108) and the Open Fund Project of Key Laboratory in Hunan Universities (No. 18K010).

References

Cang, S., Li, Y., Zhang, R. & Wang, Z. [2019] "Hidden and self-excited coexisting attractors in a Lorenz-like system with two equilibrium points," *Nonlin. Dyn.* **95**, 381–390.

Chen, G. R. & Ueta, T. [1999] "Yet another chaotic attractor," *Int. J. Bifurcation and Chaos* **9**, 1465–1466.

Chen, C., Chen, J., Bao, H., Chen, M. & Bao, B. [2019] "Coexisting multi-stable patterns in memristor synapse-coupled Hopfield neural network with two neurons," *Nonlin. Dyn.* **95**, 3385–3399.

Cheng, G. F., Wang, C. H. & Chen, H. [2019] "A novel color image encryption algorithm based on hyperchaotic system and permutation-diffusion architecture," *Int. J. Bifurcation and Chaos* **29**, 1950115-1–17.

Dadras, S., Momeni, H. R., Qi, G. & Wang, Z. L. [2012] "Four-wing hyperchaotic attractor generated from a new 4D system with one equilibrium and its fractional-order form," *Nonlin. Dyn.* **67**, 1161–1173.

Danca, M.-F., Fečkan, M., Kuznetsov, N. & Chen, G. R. [2016] "Looking more closely at the Rabinovich–Fabrikant system," *Int. J. Bifurcation and Chaos* **26**, 1650038-1–21.

Elwakil, A. S., Özogŭz, S. & Kennedy, M. P. [2003] "A four-wing butterfly attractor from a fully autonomous system," *Int. J. Bifurcation and Chaos* **13**, 3093–3098.

Jafari, S. & Sprott, J. C. [2013] "Simple chaotic flows with a line equilibrium," *Chaos Solit. Fract.* **57**, 79–84.

Jin, J. [2018] "Programmable multi-direction fully integrated chaotic oscillator," *Microelectron. J.* **75**, 27–34.

Jin, J. & Li, C. [2019] "Fully integrated memristor and its application on the scroll-controllable hyperchaotic system," *Complexity* **2019**, 410639.

Kuznetsov, N. V., Leonov, G. A. & Vagaitsev, V. I. [2010] "Analytical numerical method for attractor localization of generalized Chua's system," *IFAC Proc.* **43**, 29–33.

Leonov, G. A., Kuznetsov, N. V. & Vagaitsev, V. I. [2011] "Localization of hidden Chua's attractors," *Phys. Lett. A* **375**, 2230–2233.

Li, K., Zhao, M. & Fu, X. [2009] "Projective synchronization of driving-response systems and its application to secure communication," *IEEE Trans. Circuits Syst.-I*: *Reg. Papers* **56**, 2280–2291.

Li, C., Min, F. & Li, C. [2018a] "Multiple coexisting attractors of the serial–parallel memristor-based chaotic system and its adaptive generalized synchronization," *Nonlin. Dyn.* **94**, 2785–2806.

Li, C., Sprott, J. C., Liu, Y., Gu, Z. & Zhang, J. [2018b] "Offset boosting for breeding conditional symmetry," *Int. J. Bifurcation and Chaos* **28**, 1850163-1–13.

Li, C., Xu, Y., Chen, G. R., Liu, Y. & Zheng, J. [2019a] "Conditional symmetry: Bond for attractor growing," *Nonlin. Dyn.* **95**, 1245–1256.

Li, C., Lu, T., Chen, G. R. & Xing, H. [2019b] "Doubling the coexisting attractors," *Chaos* **29**, 051102.

Lin, H. R. & Wang, C. H. [2020] "Influences of electromagnetic radiation distribution on chaotic dynamics of a neural network," *Appl. Math. Comput.* **369**, 124840.

Liu, W. & Chen, G. R. [2003] "A new chaotic system and its generation," *Int. J. Bifurcation and Chaos* **13**, 261–267.

Liu, W. & Chen, G. R. [2004] "Can a three-dimensional smooth autonomous quadratic chaotic system generate a single four-scroll attractor?" *Int. J. Bifurcation and Chaos* **14**, 1395–1403.

Lorenz, E. N. [1963] "Deterministic nonperiodic flow," *J. Atmosph. Sci.* **20**, 130–141.

Lü, J., Chen, G. R. & Chang, D. [2004] "A new chaotic system and beyond: The generalized Lorenz-like system," *Int. J. Bifurcation and Chaos* **14**, 1507–1537.

Ma, J., Wang, L., Duan, S. & Xu, Y. [2017] "A multiwing butterfly chaotic system and its implementation," *Int. J. Circuit Th. Appl.* **25**, 1550056.

Molaie, M., Jafari, S. & Sprott, J. C. [2013] "Simple chaotic flows with one stable equilibrium," *Int. J. Bifurcation and Chaos* **23**, 1350188-1–7.

Pham, V. T., Jafari, S., Volos, C., Wang, X. & Golpayegani, S. M. R. H. [2014] "Is that really hidden? The presence of complex fixed-points in chaotic flows with no equilibria," *Int. J. Bifurcation and Chaos* **24**, 1450146-1–6.

Pham, V. T., Wang, X., Jafari, S., Volos, C. & Kapitaniak, T. [2017] "From Wang–Chen system with only one stable equilibrium to a new chaotic system without equilibrium," *Int. J. Bifurcation and Chaos* **27**, 1750097-1–9.

Qi, G., Chen, R. G., Li, S. & Zhang, Y. [2006] "Four-wing attractors: From pseudo to real," *Int. J. Bifurcation and Chaos* **16**, 859–885.

Qi, G. & Liang, X. [2017] "Mechanism and energy cycling of the Qi four-wing chaotic system," *Int. J. Bifurcation and Chaos* **27**, 1750180-1–15.

Qi, G. [2019] "Modelings and mechanism analysis underlying both the 4D Euler equations and Hamiltonian conservative chaotic systems," *Nonlin. Dyn.* **95**, 2063–2077.

Qi, G. & Yang, X. [2019] "Modeling of a chaotic gyrostat system and mechanism analysis of dynamics using force and energy," *Complexity* **2019**, 5439596.

Rössler, O. E. [1976] "An equation for continuous chaos," *Phys. Lett. A* **57**, 397–398.

Tahir, F. R., Jafari, S., Pham, V. T., Volos, C. & Wang, X. [2015] "A novel no-equilibrium chaotic system with multiwing butterfly attractors," *Int. J. Bifurcation and Chaos* **45**, 1873–1884.

Wang, X. & Chen, G. R. [2012] "A chaotic system with only one stable equilibrium," *Commun. Nonlin. Sci. Numer. Simulat.* **17**, 1264–1272.

Wang, C. H., Liu, X. M. & Xia, H. [2017a] "Multi-piecewise quadratic nonlinearity memristor and its $2N$-scroll and $2N + 1$-scroll chaotic attractors system," *Chaos* **27**, 033114.

Wang, C. H., Xia, H. & Zhou, L. [2017b] "A memristive hyperchaotic multiscroll jerk system with controllable scroll numbers," *Int. J. Bifurcation and Chaos* **27**, 1750091-1–15.

Wang, C. H., Zhou, L. & Wu, R. P. [2018] "The design and realization of a hyper-chaotic circuit based on a flux-controlled memristor with linear memductance," *J. Circuits Syst. Comput.* **27**, 1850038.

Wei, Z. & Zhang, W. [2014] "Hidden hyperchaotic attractors in a modified Lorenz–Stenflo system with only one stable equilibrium," *Int. J. Bifurcation and Chaos* **24**, 1450127-1–14.

Wei, Z., Moroz, I., Sprott, J. C., Akgul, A. & Zhang, W. [2017] "Hidden hyperchaos and electronic circuit application in a 5D self-exciting homopolar disc dynamo," *Chaos* **27**, 033101.

Yang, Q., Wei, Z. & Chen, G. R. [2010] "An unusual 3D autonomous quadratic chaotic system with two stable node-foci," *Int. J. Bifurcation and Chaos* **20**, 1061–1083.

Yao, W., Wang, C. H., Cao, J. D., Sun, Y. C. & Zhou, C. [2019] "Hybrid multisynchronization of coupled multistable memristive neural networks with time delays," *Neurocomputing* **363**, 281–294.

Yin, Q. & Wang, C. H. [2018] "A new chaotic image encryption scheme using breadth-first search and dynamic diffusion," *Int. J. Bifurcation and Chaos* **51**, 665–673.

Yu, S. M., Tang, W. S., Lü, J. H. & Chen, G. R. [2010a] "Design and implementation of multiwing butterfly chaotic attractors via Lorenz-type systems," *Int. J. Bifurcation and Chaos* **20**, 29–41.

Yu, S., Lü, J., Chen, G. R. & Yu, X. [2010b] "Design and implementation of grid multiwing butterfly chaotic attractors from a piecewise Lorenz system," *IEEE Trans. Circuits Syst.-II*: *Exp. Briefs* **57**, 803–807.

Yu, S., Lü, J., Chen, G. R. & Yu, X. [2011] "Generating grid multiwing chaotic attractors by constructing heteroclinic loops into switching systems," *IEEE Trans. Circuits Syst.-II*: *Exp. Briefs* **58**, 314–318.

Yu, S. M., Lü, J. H., Yu, X. H. & Chen, G. R. [2012] "Design and implementation of grid multiwing hyperchaotic Lorenz system family via switching control and constructing super-heteroclinic loops," *IEEE Trans. Circuits Syst.-I*: *Reg. Papers* **59**, 1015–1028.

Yu, N., Wang, Y. N., Liu, X. K. & Xiao, J. W. [2018] "3D grid multiwing chaotic attractors," *Int. J. Bifurcation and Chaos* **28**, 1850045-1–16.

Zhang, S., Zeng, Y., Li, Z., Wang, M. & Xiong, L. [2018a] "Generating one to four-wing hidden attractors in a novel 4D no-equilibrium chaotic system with extreme multistability," *Chaos* **28**, 013113.

Zhang, S., Zeng, Y. C. & Li, Z. J. [2018b] "A novel four-dimensional no-equilibrium hyper-chaotic system with grid multiwing hyper-chaotic hidden attractors," *J. Comput. Nonlin. Dyn.* **13**, 090908.

Zhang, X. & Wang, C. H. [2019a] "A novel multi-attractor period multi-scroll chaotic integrated circuit based on CMOS wide adjustable CCCII," *IEEE Access* **7**, 16336–16350.

Zhang, X. & Wang, C. H. [2019b] "Multiscroll hyperchaotic system with hidden attractors and its circuit implementation," *Int. J. Bifurcation and Chaos* **29**, 1950117-1–14.

Zhou, L., Wang, C. H. & Zhou, L. L. [2016] "Generating hyperchaotic multiwing attractor in a 4D memristive circuit," *Nonlin. Dyn.* **85**, 2653–2663.

Zhou, L., Wang, C. H. & Zhou, L. L. [2017] "Generating four-wing hyperchaotic attractor and two-wing, three-wing, and four-wing chaotic attractors in 4D memristive system," *Int. J. Bifurcation and Chaos* **27**, 1750027-1–14.

Zhou, L., Wang, C. H. & Zhou, L. L. [2018a] "A novel no-equilibrium hyperchaotic multiwing system via introducing memristor," *Int. J. Circuit Th. Appl.* **46**, 84–98.

Zhou, L., Wang, C. H. & Zhang, X. [2018b] "Various attractors, coexisting attractors and antimonotonicity in a simple fourth-order memristive twin-T oscillator," *Int. J. Bifurcation and Chaos* **28**, 1850050-1–18.

Zhou, M. J. & Wang, C. H. [2020] "A novel image encryption scheme based on conservative hyperchaotic system and closed-loop diffusion between bolcks," *Sign. Process.* **171**, 107484.